

**Weierstraß-Institut
für Angewandte Analysis und Stochastik
Leibniz-Institut im Forschungsverbund Berlin e. V.**

Preprint

ISSN 2198-5855

Polarized frequency combs in a mode-locked VECSEL

Krassimir Panajotov¹, Andrei G. Vladimirov², Mustapha Tlidi³

submitted: May 13, 2024

¹ Georgi Nadjakov Institute of Solid State Physics
Bulgarian Academy of Sciences
72 Tzarigradsko Chaussee blvd.
1784 Sofia
Bulgaria
and
Vrije Universiteit Brussel
Pleinlaan 2
1050 Brussels
Belgium
E-mail: kpan@issp.bas.bg

² Weierstrass Institute
Mohrenstr. 39
10117 Berlin
Germany
E-Mail: andrei.vladimirov@wias-berlin.de

³ Département de Physique
Faculté des Sciences
Université libre de Bruxelles
Boulevard du Triomphe
1050 Brussels
Belgium
E-Mail: mtlidi@ulb.ac.be

No. 3109
Berlin 2024



2020 *Mathematics Subject Classification.* 78A60, 37N20, 34K99.

2010 *Physics and Astronomy Classification Scheme.* 42.65.-k, 42.55.Px, 42.60.Fc, 42.25.Ja.

Key words and phrases. Vertical cavity surface emitting lasers, mode-locking, polarization dynamics, optical frequency combs.

A.V. acknowledges the financial support of the Deutsche Forschungsgemeinschaft (DFG Project No. 491234846). M.T. is a Research Director at Fonds de la Recherche Scientifique FNRS.

Edited by
Weierstraß-Institut für Angewandte Analysis und Stochastik (WIAS)
Leibniz-Institut im Forschungsverbund Berlin e. V.
Mohrenstraße 39
10117 Berlin
Germany

Fax: +49 30 20372-303
E-Mail: preprint@wias-berlin.de
World Wide Web: <http://www.wias-berlin.de/>

Polarized frequency combs in a mode-locked VECSEL

Krassimir Panajotov, Andrei G. Vladimirov, Mustapha Tlidi

Abstract

In this paper, we present a detailed and rigorous derivation of the delay differential equations of the spin-flip model for vertical external cavity lasers with a semiconductor saturable absorption mirror. This model describes mode-locked semiconductor lasers in the ring-resonator geometry with unidirectional lasing. This contribution completes a previous communication [Vladimirov et al. Opt. Lett., 45, 252 (2020)], and we further complete the analytical derivation by taking into account phase and amplitude anisotropies and the resulting different delay times for orthogonal linear polarizations. We show evidence of the coexistence of two linearly polarized frequency combs generation with slightly different repetition rates due to the birefringence-induced time-of-flight difference.

1 Introduction

Vertical External-Cavity Surface-Emitting Lasers (VECSELs), first developed in 1997 [1], are of great interest in the scientific community thanks to the possibility of output power scalability, wavelength flexibility, and Optical Frequency Combs (OFC) generation. Semiconductor lasers with saturable absorber section are widely used to generate short pulses by mode locking [2]. Passive mode locking was first demonstrated in a VECSEL with a Semiconductor Saturable Absorption Mirror (SESAM), resulting in the generation of a ps pulse train with a GHz repetition rate [3]. Since then, much progress has been made towards higher intensity pulses with shorter duration [4, 5, 6, 7]. Two orthogonally polarized OFCs with different pulse repetition rates have been demonstrated by using a birefringent crystal in the external cavity to split the laser emission into two spots on the chip combining the gain and saturable absorption media [8]. In [9] two orthogonally polarized OFCs were theoretically demonstrated for a VECSEL with SESAM and complex dynamics, including polarization chaotic dynamics was predicted. Recently, a thorough experimental investigation of polarization dynamics of a VECSEL mode-locked with SESAM has been performed [10]. Acquiring temporal traces of polarization resolved intensities provided the Stokes parameters dynamics and demonstrated that the polarization of the generated light changes during the pulse is generally elliptical with significant s_3 Stokes parameter.

Such unusual polarization dynamics is well known for Vertical-Cavity Surface-Emitting Lasers (VCSELs) [11, 12, 13] (for a review see [14]). It can lead to deterministic polarization chaos in a solitary laser [15] or a laser subject to optical feedback [16] or injection [17], vector cavity solitons [18] and period doubling route to spatially localized chaos of elliptically polarized cavity solitons [19] in broad-area VCSELs, as well as to ultrahigh-frequency oscillations [20]. It arises due to the lack of strong polarization selectivity mechanism: the cylindrical symmetry removes the waveguiding and reflectivity anisotropies and the surface emission removes the gain anisotropy [21, 22]. Since the same surface emission and absorption occur in the gain and SESAM chips of VECSELs, complex polarization dynamics should also occur with the same origin as in VCSELs.

A well-accepted model that reproduces these intriguing polarization dynamics is the so called Spin-Flip Model or SFM [21]. The SFM considers the transitions between the conduction band and heavy hole valence band in a quantum well active material as two two-level systems with different spin orientations that are coupled by the spin-flip processes. It takes into account the carrier spin dynamics occurring on a time scale of hundreds of ps , an intermediate time scale between the photon lifetime (several ps) and the carrier lifetime (ns). Taking into account the VCSEL phase and amplitude

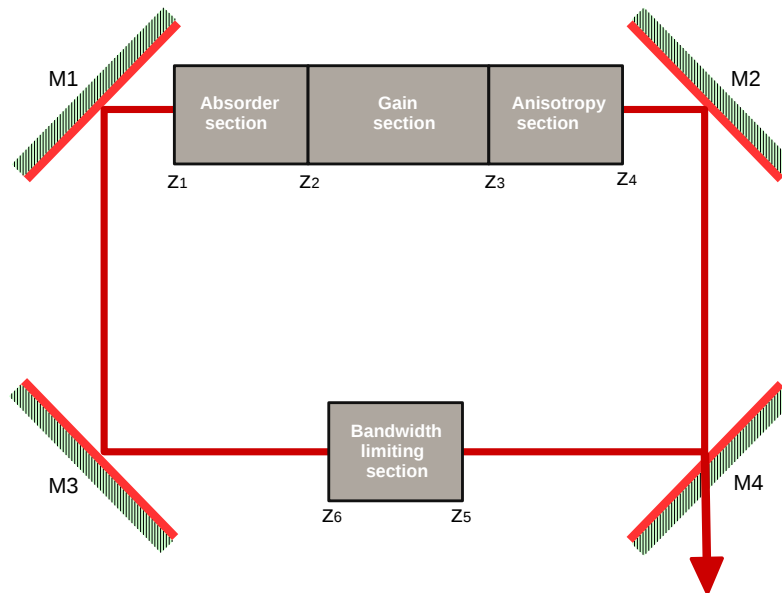


Figure 1: (color online) The schematic setup of a unidirectional ring resonator produces passively mode-locked semiconductor lasers filled with four sections along the optical axis, i.e., the z coordinate. The absorbing section $z_1 < z < z_2$, the gain section $z_2 < z < z_3$, the spectral filtering section $z_3 < z < z_4$, and the anisotropic section $z_5 < z < z_6$. The mirrors $M_{1,2,3}$ are fully reflective, while M_4 is the output mirror, which is partially reflective.

anisotropies (birefringence and dichroism), the SFM has explained the polarization switching between two linearly polarized (LP) fundamental transverse modes with injection current as a phase instability due to amplitude-phase coupling mediated by the linewidth enhancement factor in the semiconductor active medium [22] (for a review see [14]). It further predicted complex polarization dynamics even in a solitary VCSEL, such a period-doubling route to chaotic dynamics has been experimentally confirmed in [15].

For the case of spatial solitons in broad-area VCSELs, the SFM explained the orthogonally polarized localized structures found in [23] and the vector character of the solitons found in [18]. Recently, multistability and complex polarization dynamics of an isolated localized structure have been predicted by SFM for a VCSEL with a saturable absorber section [19]. SFM also explains the appearance of ultra-fast polarization oscillations [20]. Time-delayed SFM for VCSELs with SA-mirror has recently been introduced in [9] based on an extension of the delay differential equations (DDEs) proposed in [24]. It numerically demonstrated the generation of either x- or y-linearly polarized pulse trains in the fundamental mode-locked regime or in a regime of more than one pulse per roundtrip, as well as more complicated two-polarization mode dynamics with increasing the pump power.

This paper is organized as follows. After an introduction, we present in detail the spin-flip model delay differential equation model for vertical external cavity lasers with a saturable semiconductor absorption mirror (Sec. II). This differential equation model, which describes mode-locked semiconductor lasers, assumes a ring resonator geometry with a unidirectional laser (see Fig. 1). First, we consider the phase and amplitude anisotropies and the resulting different delay times for orthogonal linear polarizations - the derivation of the anisotropy matrix is presented in subsection A. After describing the field equations assuming the slowly varying envelope approximation (subsection B), we derive the carrier equation (subsection C). The final section is devoted to the numerical integration of the derived model equations (Sec. III). We demonstrate the generation of two coexisting linearly polarized frequency combs with slightly different repetition rates due to the birefringence-induced time-of-flight difference. We conclude

in sec. IV.

2 Spin-flip delay-differential equation model for mode-locked VECSEL

We consider a ring-cavity geometry with unidirectional lasing containing gain and absorber sections in VECSELs, the spectral filtering, and the anisotropic section as depicted in Fig. 1. The delay differential equations (DDEs) are a well-known model for describing mode-locked semiconductor lasers with a saturable absorber, as shown by Vladimirov and Turaev in [24]. In the absence of spectral filtering and anisotropy, the gain and absorber sections in VECSELs are described by the spin flip model [21] with spatial derivatives included and linear loss excluded. Under these modifications, the time evolution of the right-left amplitude of the field associated with circular polarization and the carriers reads

$$\partial_z A^\pm + \partial_t A^\pm = (1 - i\alpha)(N \pm n)A^\pm/2, \quad (1)$$

$$\partial_t N = N_0 - \gamma_e N - s|A^+|^2(N + n) - s|A^-|^2(N - n), \quad (2)$$

$$\partial_t n = n_0 - \gamma_s n - s|A^+|^2(N + n) + s|A^-|^2(N - n). \quad (3)$$

Here A^\pm are the slowly varying envelope field amplitudes for the right (+) and left (−) circular polarization. The variables N and n represent the overall and excess carrier densities, i.e., the half sum and the half difference of the carrier densities of the two-level systems with different spin orientations [21]. They are rescaled so that the multiplier in the field equations becomes $1/2$. The parameters $\alpha = \alpha_g$ and $\alpha = \alpha_q$ are the linewidth enhancement factors, $\gamma_e = \gamma_g$ and $\gamma_e = \gamma_q$ are the carrier density relaxation rates, $\gamma_s = \gamma_{sh}$ and $\gamma_s = \gamma_{sp}$ are the spin-flip relaxation rates in the gain and SA sections, respectively. N_0 and n_0 are the pump and unsaturated absorption parameters for the overall and excess carrier densities, respectively. The parameter s in Eqs. (2) and (3) is the ratio of the saturation intensities in the gain and absorber sections. $s = 1$ for the gain section and $s = (g_q \Gamma_q)/(g_g \Gamma_g)$ for the absorber section, where g_g (g_q) and Γ_g (Γ_q) are the differential gains and confinement factors in the gain (absorber) section.

2.1 Anisotropy matrix

The anisotropy matrix \tilde{M} is obtained from the equations for the anisotropic section as included phenomenologically in the Spin-Flip Model [22]

$$\begin{aligned} (\partial_z + \partial_t)A^+ &= -(\gamma_a + i\gamma_p)A^-/2 \\ (\partial_z + \partial_t)A^- &= -(\gamma_a + i\gamma_p)A^+/2, \end{aligned} \quad (4)$$

where γ_a and γ_p represent the amplitude and phase anisotropies [22]. Taking the sum and the difference for right and left circularly polarized light in Eq. (4)

$$\begin{aligned} (\partial_z + \partial_t)(A^+ + A^-) &= -(\gamma_a + i\gamma_p)(A^+ + A^-)/2, \\ (\partial_z + \partial_t)(A^+ - A^-) &= (\gamma_a + i\gamma_p)(A^+ - A^-)/2. \end{aligned}$$

with solution in terms of LP states

$$\begin{aligned} A_x^{(4)}(t) &= e^{-(\gamma_a + i\gamma_p)t_3/2} A_x^{(3)}(t - t_3 - \delta t), \\ A_y^{(4)}(t) &= e^{(\gamma_a + i\gamma_p)t_3/2} A_y^{(3)}(t - t_3 + \delta t), \end{aligned} \quad (5)$$

where $A_x^{(k)}(t) = A_x(z_k, t)$ with $k = 3, 4$, $l_3 = z_4 - z_3$ and t_3 is the delay time due to the light propagation in the anisotropy section with δt the difference due to the birefringence. The anisotropy matrix \tilde{M} becomes

$$\tilde{M} = \begin{bmatrix} e^{-(\tilde{\gamma}_a + i\tilde{\gamma}_p)} & 0 \\ 0 & e^{\tilde{\gamma}_a + i\tilde{\gamma}_p} \end{bmatrix}. \quad (6)$$

where $\tilde{\gamma}_p = \gamma_p l_3/2$ and $\tilde{\gamma}_a = \gamma_a l_3/2$ with $l_3 = z_4 - z_3$ being the length of the anisotropic section.

2.2 Field equations

Integrating the field equations (1) along the characteristics, we get

$$\begin{pmatrix} A_3^+(t) \\ A_3^-(t) \end{pmatrix} = e^{i\phi_2} \begin{pmatrix} e^{(1-i\alpha_g)(g+h)/2} A_2^+(t-t_2) \\ e^{(1-i\alpha_g)(g-h)/2} A_2^-(t-t_2) \end{pmatrix}, \quad (7)$$

$$\begin{pmatrix} A_2^+(t) \\ A_2^-(t) \end{pmatrix} = e^{i\phi_1} \begin{pmatrix} e^{-(1-i\alpha_q)(q+p)/2} A_1^+(t-t_1) \\ e^{-(1-i\alpha_q)(q-p)/2} A_1^-(t-t_1) \end{pmatrix}, \quad (8)$$

where $A_k^\pm(t) = A^\pm(z_k, t)$, $g(t) = \int_{z_2}^{z_3} N(z, t) dz$ and $h(t) = \int_{z_2}^{z_3} n(x, t) dz$ for the gain section and $q(t) = -\int_{z_1}^{z_2} N dz$ and $p(t) = -\int_{z_1}^{z_2} n dz$ for the SA section. The delay times, denoted as $t_{1,2}$, and phase shifts, represented by $\phi_{1,2}$, arise from the propagation through the absorber and gain media. Taking the sum and the difference of the two rows of Eq. (7), we obtain

$$\begin{pmatrix} A_3^+(t) + A_3^-(t) \\ A_3^+(t) - A_3^-(t) \end{pmatrix} = e^{(1-i\alpha_g)g/2 + i\phi_2} \times \begin{pmatrix} A_2^+(t-t_2)e^{(1-i\alpha_g)h/2} + A_2^-(t-t_2)e^{-(1-i\alpha_g)h/2} \\ A_2^+(t-t_2)e^{(1-i\alpha_g)h/2} - A_2^-(t-t_2)e^{-(1-i\alpha_g)h/2} \end{pmatrix}. \quad (9)$$

Similarly, if we take the sum and the difference of the two rows of Eq. (8), we obtain

$$\begin{pmatrix} A_2^+(t) + A_2^-(t) \\ A_2^+(t) - A_2^-(t) \end{pmatrix} = e^{-(1-i\alpha_q)q/2 + i\phi_1} \times \begin{pmatrix} e^{-(1-i\alpha_q)p/2} A_1^+(t-t_1) + e^{(1-i\alpha_q)p/2} A_1^-(t-t_1) \\ e^{-(1-i\alpha_q)p/2} A_1^+(t-t_1) - e^{(1-i\alpha_q)p/2} A_1^-(t-t_1) \end{pmatrix}. \quad (10)$$

Using $e^{\pm x} = ch(x) \pm sh(x)$ in Eqns. (9), we obtain

$$\begin{pmatrix} A_3^+(t) + A_3^-(t) \\ A_3^+(t) - A_3^-(t) \end{pmatrix} = e^{(1-i\alpha_g)g/2 + i\phi_2} \times \left[\begin{pmatrix} [A_2^+(t-t_2) + A_2^-(t-t_2)] \cosh [(1-i\alpha_g)h/2] \\ [A_2^+(t-t_2) - A_2^-(t-t_2)] \cosh [(1-i\alpha_g)h/2] \end{pmatrix} + \begin{pmatrix} [A_2^+(t-t_2) - A_2^-(t-t_2)] \sinh [(1-i\alpha_g)h/2] \\ [A_2^+(t-t_2) + A_2^-(t-t_2)] \sinh [(1-i\alpha_g)h/2] \end{pmatrix} \right]. \quad (11)$$

Using the same substitution for $e^{\pm x}$ in Eqns. (10), we obtain

$$\begin{pmatrix} A_2^+(t) + A_2^-(t) \\ A_2^+(t) - A_2^-(t) \end{pmatrix} = e^{-(1-i\alpha_q)q/2 + i\phi_1} \times \left[\begin{pmatrix} [A_1^+(t-t_1) + A_1^-(t-t_1)] \cosh [(1-i\alpha_q)p/2] \\ [A_1^+(t-t_1) - A_1^-(t-t_1)] \cosh [(1-i\alpha_q)p/2] \end{pmatrix} - \begin{pmatrix} [A_1^+(t-t_1) - A_1^-(t-t_1)] \sinh [(1-i\alpha_q)p/2] \\ [A_1^+(t-t_1) + A_1^-(t-t_1)] \sinh [(1-i\alpha_q)p/2] \end{pmatrix} \right]. \quad (12)$$

We may now rewrite the last two equations, Eq. (11) and Eq. (12) in terms of the orthogonal linear components of the electric field by utilizing the relations $A_x^{(k)} = (A_k^+ + A_k^-)/\sqrt{2}$ and $A_y^{(k)} = -i(A_k^+ - A_k^-)/\sqrt{2}$, i.e.

$$\begin{pmatrix} A_x^{(3)}(t) \\ iA_y^{(3)}(t) \end{pmatrix} = e^{(1-i\alpha_g)g/2+\phi_2} \left[\begin{pmatrix} A_x^{(2)}(t-t_2) \cosh[(1-i\alpha_g)h/2] \\ iA_y^{(2)}(t-t_2) \cosh((1-i\alpha_g)h/2) \end{pmatrix} + \begin{pmatrix} iA_y^{(2)}(t-t_2) \sinh[(1-i\alpha_g)h/2] \\ A_x^{(2)}(t-t_2) \sinh[(1-i\alpha_g)h/2] \end{pmatrix} \right], \quad (13)$$

and

$$\begin{pmatrix} A_x^{(2)}(t) \\ iA_y^{(2)}(t) \end{pmatrix} = e^{-(1-i\alpha_q)q/2+\phi_1} \left[\begin{pmatrix} A_x^{(1)}(t-t_1) \cosh[(1-i\alpha_q)p/2] \\ iA_y^{(1)}(t-t_1) \cosh[(1-i\alpha_q)p/2] \end{pmatrix} - \begin{pmatrix} iA_y^{(1)}(t-t_1) \sinh[(1-i\alpha_q)p/2] \\ A_x^{(1)}(t-t_1) \sinh[(1-i\alpha_q)p/2] \end{pmatrix} \right]. \quad (14)$$

Substituting Eq. (14) into Eq. (13) and denoting $(1-i\alpha_g)h/2 \rightarrow \tilde{h}$, $(1-i\alpha_q)p(t-t_2)/2 \rightarrow \tilde{p}$, and $q(t-t_2) \rightarrow \tilde{q}$ we obtain

$$\begin{pmatrix} A_x^{(3)}(t) \\ A_y^{(3)}(t) \end{pmatrix} = e^{(1-i\alpha_g)g/2-(1-i\alpha_q)\tilde{q}/2+i(\phi_1+\phi_2)} \times \begin{pmatrix} \tilde{A}_x^{(2)}(t-t_2) \cosh(\tilde{h}) + i\tilde{A}_y^{(2)}(t-t_2) \sinh(\tilde{h}) \\ \tilde{A}_y^{(2)}(t-t_2) \cosh(\tilde{h}) - i\tilde{A}_x^{(2)}(t-t_2) \sinh(\tilde{h}) \end{pmatrix}, \quad (15)$$

with

$$\begin{aligned} \tilde{A}_x^{(2)}(t) &= A_x^{(1)}(t-t_1) \cosh(\tilde{p}) - iA_y^{(1)}(t-t_1) \sinh(\tilde{p}), \\ \tilde{A}_y^{(2)}(t) &= A_y^{(1)}(t-t_1) \cosh(\tilde{p}) + iA_x^{(1)}(t-t_1) \sinh(\tilde{p}). \end{aligned}$$

Performing the algebraic calculations in Eq. (15) we obtain

$$\begin{pmatrix} A_x^{(3)}(t) \\ A_y^{(3)}(t) \end{pmatrix} = e^{(1-i\alpha_g)g/2-(1-i\alpha_q)\tilde{q}/2} \times \begin{pmatrix} A_x^{(1)}(t-t_{12}) \cosh(\tilde{p}-\tilde{h}) - iA_y^{(1)}(t-t_{12}) \sinh(\tilde{p}-\tilde{h}) \\ A_y^{(1)}(t-t_{12}) \cosh(\tilde{p}-\tilde{h}) + iA_x^{(1)}(t-t_{12}) \sinh(\tilde{p}-\tilde{h}) \end{pmatrix}, \quad (16)$$

where $t_{12} = t_1 + t_2$.

Using Eq. (16) together with Eq. (5) and the relations $A_{x,y}^{(1)}(t) = e^{i\phi_0} A_{x,y}^{(0)}(t-t_0)$, $A_{x,y}^{(5)}(t) = \sqrt{\kappa} e^{i\phi_4} A_{x,y}^{(4)}(t-t_4)$ where, κ is the round-trip intensity attenuation factor, and $\gamma^{-1} \partial_t A_{x,y}^{(0)}(t) +$

$A_{x,y}^{(0)}(t) = A_{x,y}^{(5)}(t)$, which defines a Lorentzian spectral filter with the bandwidth γ describing the overall spectral filtering including the dispersion of material gain, SA subcavities, and distributed Bragg reflectors, we get the final equation for the field envelopes:

$$\gamma^{-1} \frac{d}{dt} \begin{pmatrix} A_x \\ A_y \end{pmatrix} + \begin{pmatrix} A_x \\ A_y \end{pmatrix} = \sqrt{\kappa} \tilde{M} \times \begin{pmatrix} R_+ [A_x(t - T_+) \cosh(\Psi_+) - iA_y(t - T_+) \sinh(\Psi_+)] \\ R_- [A_y(t - T_-) \cosh(\Psi_-) + iA_x(t - T_-) \sinh(\Psi_-)] \end{pmatrix}, \quad (17)$$

$$R_{\pm} = e^{(1-i\alpha_g)G(t-T_{\pm})/2 - (1-i\alpha_q)Q(t-T_{\pm})/2 + i\phi}, \quad (18)$$

$$\Psi_{\pm} = (1 - i\alpha_g)P(t - T_{\pm})/2 - (1 - i\alpha_q)H(t - T_{\pm})/2, \quad (19)$$

where $A_{x,y}(t) = A_{x,y}^{(0)}(t) \equiv A_{x,y}(z_0, t)$, $\phi = \sum_{k=0}^4 \phi_k$ is the total phase shift per round-trip, $T_{\pm} = \pm\delta t + \sum_{k=0}^4 t_k$ are the cold cavity round trip times for the two polarizations, $G = g(t + t_0 + t_1 + t_2)$, $Q = q(t + t_0 + t_1)$, $P(t) = p(t + t_0 + t_1)$ and $H(t) = h(t + t_0 + t_1 + t_2)$.

2.3 Carrier equations

Without loss of generality, we assume that the field envelope is rescaled so that the saturation parameter in the gain (absorber) medium is equal to unity (s). Integrating the carrier equations, Eq. (2) and Eq. (3) along z in the gain and saturable absorber sections as in [9], we obtain

$$\partial_t g = G_0 - \gamma_g g - \int_{z_2}^{z_3} |A^+|^2 (N + n) dz - \int_{z_2}^{z_3} |A^-|^2 (N - n) dz, \quad (20)$$

$$\partial_t h = H_0 - \gamma_{sg} h - \int_{z_2}^{z_3} |A^+|^2 (N + n) dz - \int_{z_2}^{z_3} |A^-|^2 (N - n) dz, \quad (21)$$

$$\partial_t q = Q_0 - \gamma_q q - s \int_{z_1}^{z_2} |A^+|^2 (N + n) dz - s \int_{z_1}^{z_2} |A^-|^2 (N - n) dz, \quad (22)$$

$$\partial_t p = P_0 - \gamma_{sq} p - s \int_{z_1}^{z_2} |A^+|^2 (N + n) dz + s \int_{z_1}^{z_2} |A^-|^2 (N - n) dz. \quad (23)$$

Now using Eq. (1) we get

$$(\partial_z + \partial_t) |A^{\pm}|^2 = A^{\pm*} (\partial_z A^{\pm} + \partial_t A^{\pm}) + A^{\pm} (\partial_z A^{\pm*} + \partial_t A^{\pm*}),$$

i.e.,

$$(\partial_z + \partial_t) |A^{\pm}|^2 = |A^{\pm}|^2 (N \pm n), \quad (24)$$

Integrating these equations along the characteristic we get

$$\int_{z_k}^{z_{k+1}} |A^{\pm}|^2 (N \pm n) dz = |A_{k+1}^{\pm}(t)|^2 - |A_k^{\pm}(t - t_k)|^2,$$

where $A_k^\pm(t) = A^\pm(z_k, t)$ and $k = 1, 2$. Expressing $A_k^\pm(t)$ in terms of $A_0^\pm(t) = A^\pm(z_0, t)$ we get

$$\begin{aligned} \int_{z_1}^{z_2} |A^\pm|^2 (N \pm n) dz &= (e^{-(q\pm p)} - 1) |A_0^\pm(t - t_0 - t_1)|^2, \\ \int_{z_2}^{z_3} |A^\pm|^2 (N \pm n) dz &= \\ e^{-(q\pm p)} (e^{(g\pm h)} - 1) |A_0^\pm(t - t_0 - t_1 - t_2)|^2, \end{aligned} \quad (25)$$

Next, instead of (20)-(23) we write the equations for $G(t) = g(t + t_0 + t_1 + t_2)$, $H(t) = h(t + t_0 + t_1 + t_2)$, $Q(t) = g(t + t_0 + t_1)$, and $P(t) = p(t + t_0 + t_1)$. Then taking into account Eq. (25) we obtain:

$$\begin{aligned} \frac{dG}{dt} &= G_0 - \gamma_g G - e^{-Q-P} (e^{G+H} - 1) |A^+(t)|^2 \\ &\quad - e^{-Q+P} (e^{G-H} - 1) |A^-(t)|^2, \\ \frac{dH}{dt} &= H_0 - \gamma_{sh} H - e^{-Q-P} (e^{G+H} - 1) |A^+(t)|^2 \\ &\quad + e^{-Q+P} (e^{G-H} - 1) |A^-(t)|^2, \\ \frac{dQ}{dt} &= Q_0 - \gamma_q Q - s(1 - e^{-Q-P}) |A^+(t)|^2 \\ &\quad - s(1 - e^{-Q+P}) |A^-(t)|^2, \\ \frac{dP}{dt} &= P_0 - \gamma_{sp} P - s(1 - e^{-Q-P}) |A^+(t)|^2 + \\ &\quad s(1 - e^{-Q+P}) |A^-(t)|^2. \end{aligned}$$

Expressing the circularly polarized light intensities in terms of the LP amplitudes A_x and A_y and carrying out the algebra we obtain

$$\begin{aligned} \frac{dG}{dt} &= G_0 - \gamma_g G - e^{-Q} [e^G \cosh(H - P) - \cosh(P)] \times \\ &\quad (|A_x|^2 + |A_y|^2) - e^{-Q} [e^G \sinh(H - P) + \sinh(P)] \times \\ &\quad i(A_x^* A_y - A_x A_y^*), \end{aligned} \quad (26)$$

$$\begin{aligned} \frac{dH}{dt} &= H_0 - \gamma_{sh} H - e^{-Q} [e^G \sinh(H - P) + \sinh(P)] \times \\ &\quad (|A_x|^2 + |A_y|^2) - e^{-Q} [e^G \cosh(H - P) - \cosh(P)] \times \\ &\quad i(A_x^* A_y - A_x A_y^*), \end{aligned} \quad (27)$$

$$\begin{aligned} \frac{dQ}{dt} &= Q_0 - \gamma_q Q - s [1 - e^{-Q} \cosh(P)] (|A_x|^2 + |A_y|^2) - \\ &\quad s e^{-Q} \sinh(P) i(A_x^* A_y - A_x A_y^*), \end{aligned} \quad (28)$$

$$\begin{aligned} \frac{dP}{dt} &= P_0 - \gamma_{sp} P - s e^{-Q} \sinh(P) (|A_x|^2 + |A_y|^2) - \\ &\quad s [1 - e^{-Q} \cosh(P)] i(A_x^* A_y - A_x A_y^*), \end{aligned} \quad (29)$$

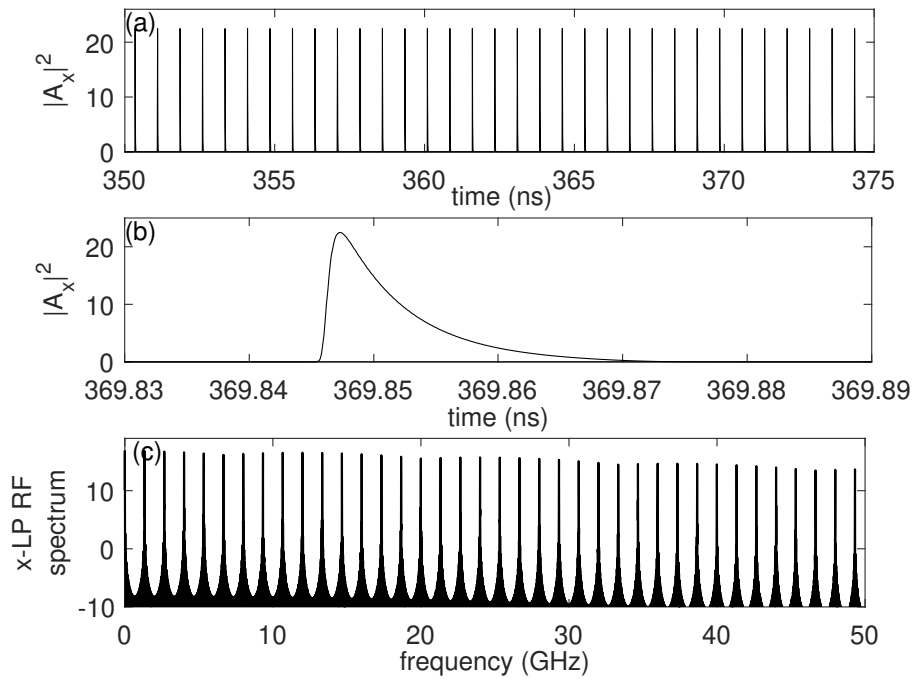


Figure 2: (a) Time trace of the intensity of x linearly polarized light; (b) time trace of a single pulse and (c) RF spectrum corresponding to a frequency comb with line spacing of 1.33 GHz. VECSEL parameters are $\gamma = 33.3$, $\gamma_g = 1.33 \times 10^{-2}$, $\gamma_q = 0.5$, $\gamma_{sh} = 0.5$, $\gamma_{sp} = 5$, $g_0 = 0.01$, $q_0 = 0.3$, $h_0 = 0$, $p_0 = 0$, $s = 25$. The VECSEL is considered isotropic, i. e. $\tilde{\gamma}_p = 0$, $\tilde{\gamma}_a = 0$ and $\tau_x = \tau_y = 75$. Initial conditions are $A_x = 0.1$, $A_y = 0$.

3 Numerical results

We integrate numerically the Eqs. (17) - (29) by using the 5th order Runge-Kutta integration scheme and accounting for the delay terms. We fix the VECSEL parameters as in [9], namely $\gamma = 33.3$, $\gamma_g = 1.33 \times 10^{-2}$, $\gamma_q = 0.5$, $\gamma_{sh} = 0.5$, $\gamma_{sp} = 5$, $g_0 = 0.01$, $q_0 = 0.3$, $h_0 = 0$, $p_0 = 0$, and $s = 25$. However, we consider a longer external cavity length of 22.5 cm, corresponding to a normalized delay time of 75. The linewidth enhancement factors are taken as $\alpha_g = \alpha_q = 0$.

First, we confirm the results of [9] namely, that for isotropic VECSEL, i.e., $\tilde{\gamma}_p = 0$ and $\tilde{\gamma}_a = 0$, and depending on which x or y linearly polarized light is chosen as an initial condition the mode locking occurs in the same LP mode. Fig. 2, calculated for initial conditions for the amplitudes of the x and y polarizations of $A_x = 0.1$ and $A_y = 0$, represents the case of mode-locked pulses in only x polarization while y polarization is not lasing. Fig. 2(a) shows a time trace of the x-LP intensity; Fig. 2(b) shows a time trace of a single pulse and Fig. 2(c) shows the RF spectrum corresponding to a frequency comb with line spacing of 1.33 GHz.

Which polarization lases for the case of isotropic VECSEL is determined by the initial conditions. For example, for initial conditions for the amplitudes of the x and y polarizations of $A_x = 0$ and $A_y = 0.1$ mode-locked pulses for y polarization are only generated (not shown). When the two LP are chosen with the same amplitude initially, the VECSEL pulsates in both polarizations simultaneously with the same pulse amplitudes - see Fig. 3 for initial conditions of $A_x = 0.1$ and $A_y = 0.1$. Fig. 3(a) and (b) shows the time traces of the intensities of x and y linear polarizations, respectively and Fig. 3(c) shows the time traces of overall carrier densities: G in the gain section (red color) and Q in the saturable absorber section (blue color). For isotropic VECSEL considered the excess carrier densities

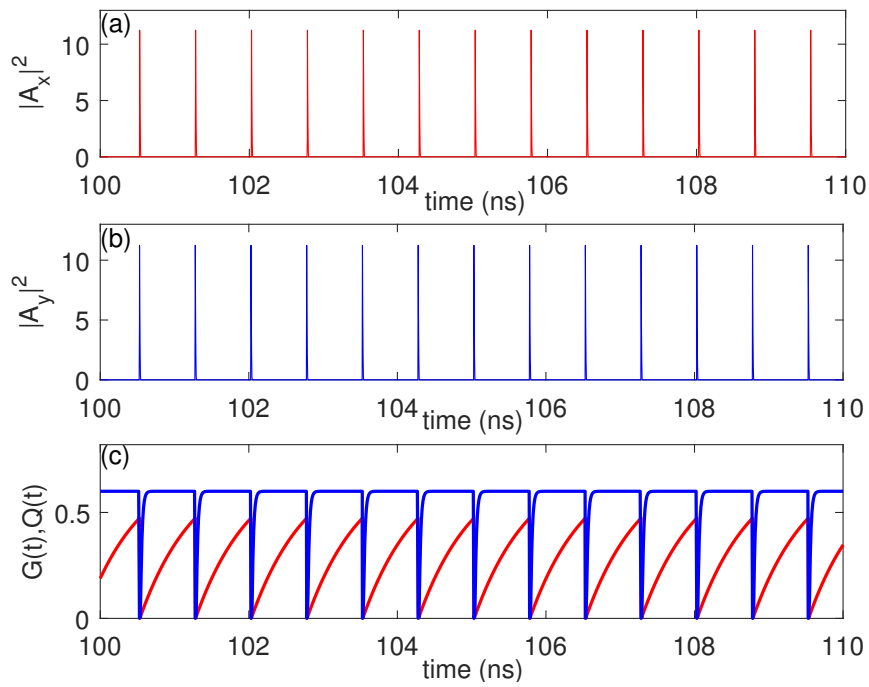


Figure 3: (color online) VECSEL with the same parameters as in Fig. 2 and initial conditions of $A_x = 0.1$ and $A_y = 0.1$. (a) Time traces of the intensities of x (red color) and y (blue color) linear polarizations and (b) time traces of overall carrier densities: G in the gain section (red color) and Q in the saturable absorber section (blue color).

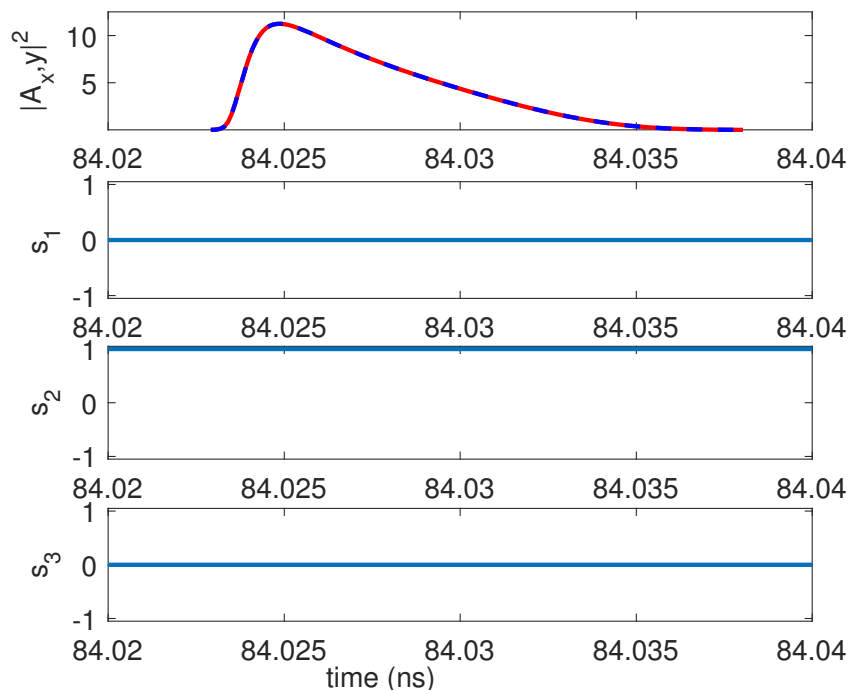


Figure 4: (color online) Evolution of the light polarization during a mode-locked pulse: (a) time traces of the intensities of x (red color) and y (blue color) linear polarizations; (b), (b) and (c) time traces of normalized Stokes parameters s_1 , s_2 and s_3 .

H in the gain section and P in the absorber sections are equal to zero.

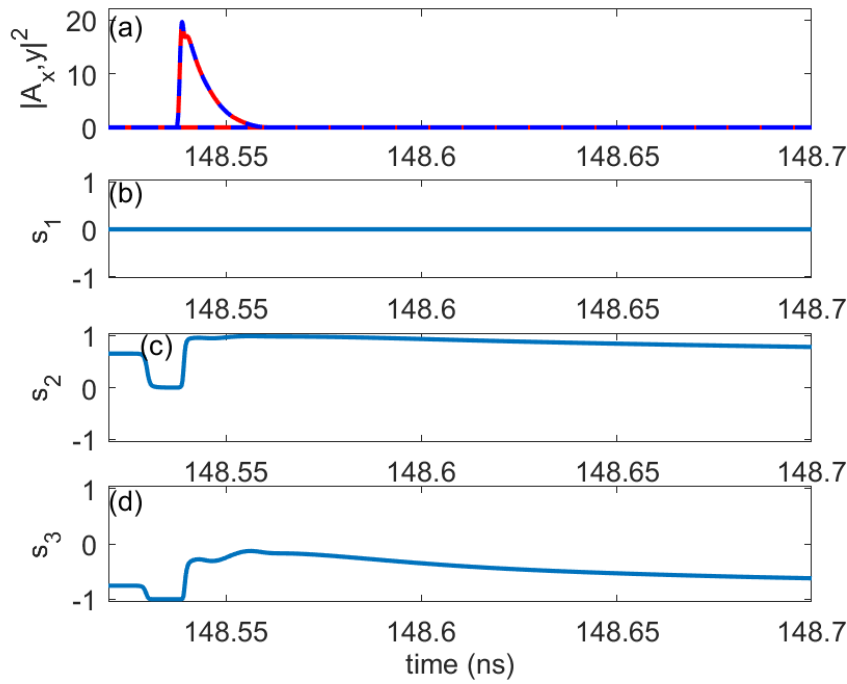


Figure 5: (color online) Evolution of the light polarization during a mode-locked pulse: (a) time traces of the intensities of x (red color) and y (blue color) linear polarizations; (b), (b) and (c) time traces of normalized Stokes parameters s_1 , s_2 and s_3 .

The evolution of the light polarization during the mode-locked pulses is illustrated in Fig. 4 by following the evolution of the Stokes parameters. As can be seen from this figure, light polarizations is not changed by mode-locking. This is because the light polarization remains linear at 45 degrees as the normalized Stokes parameter does not change $s_2 = 1$ while s_1 and s_3 are always equal to zero. However, this is not generally true: polarization of the mode-locked pulses should also depend on the polarization of the pump. In general, the VECSEL gain chip could be also not isotropically pumped, i.e. there could be an excess of one circularly polarized components of the pump. We characterized the degree of circular polarization of the pump by the parameter (see also [25, 26])

$$D_{cp} = \frac{H_0}{G_0}. \quad (30)$$

The evolution of the Stokes parameters of the light mode-locked pulses is illustrated for this case in Fig. 5 for the same parameters as in Fig 3 except that $D_{cp} = 0.025$, i.e. $H_0 = 0.0025$. As can be seen from this figure, light polarizations is now changed by the mode-locking: while $s_1 = 0$ always, s_2 and s_3 are impacted. Before the arrival of the pulse their values are $s_2 = 0.65$ and $s_3 = -0.75$ indicating elliptical polarization. Shortly before arriving of the pulse s_2 decreases abruptly to 0 and s_3 to -1 , i.e. light is circularly polarized. During the leading edge of the pulse they again change abruptly: to almost 1 and 0, respectively, indicating linear polarization at 45 degrees. During the trailing edge of the pulse and afterwards s_2 and s_3 slowly relax back to the values characteristic for the beginning of the pulse.

Fig. 6 presents a bifurcation diagram as a function of the gain chip pump G_0 for VECSEL with the same parameters as in Fig. 2. It presents the maxima and the minima of the polarization resolved intensities for the last 10 ns for a number of time traces with a duration of 150 ns starting at $G_0 = 0.001$ with initial conditions of $A_x = 0.1$ and $A_y = 0.1$ and increasing G_0 with steps of $\Delta G = 0.001$. Typical mode locking as presented so far and with progressively increasing with G_0 pulse amplitude occurs in

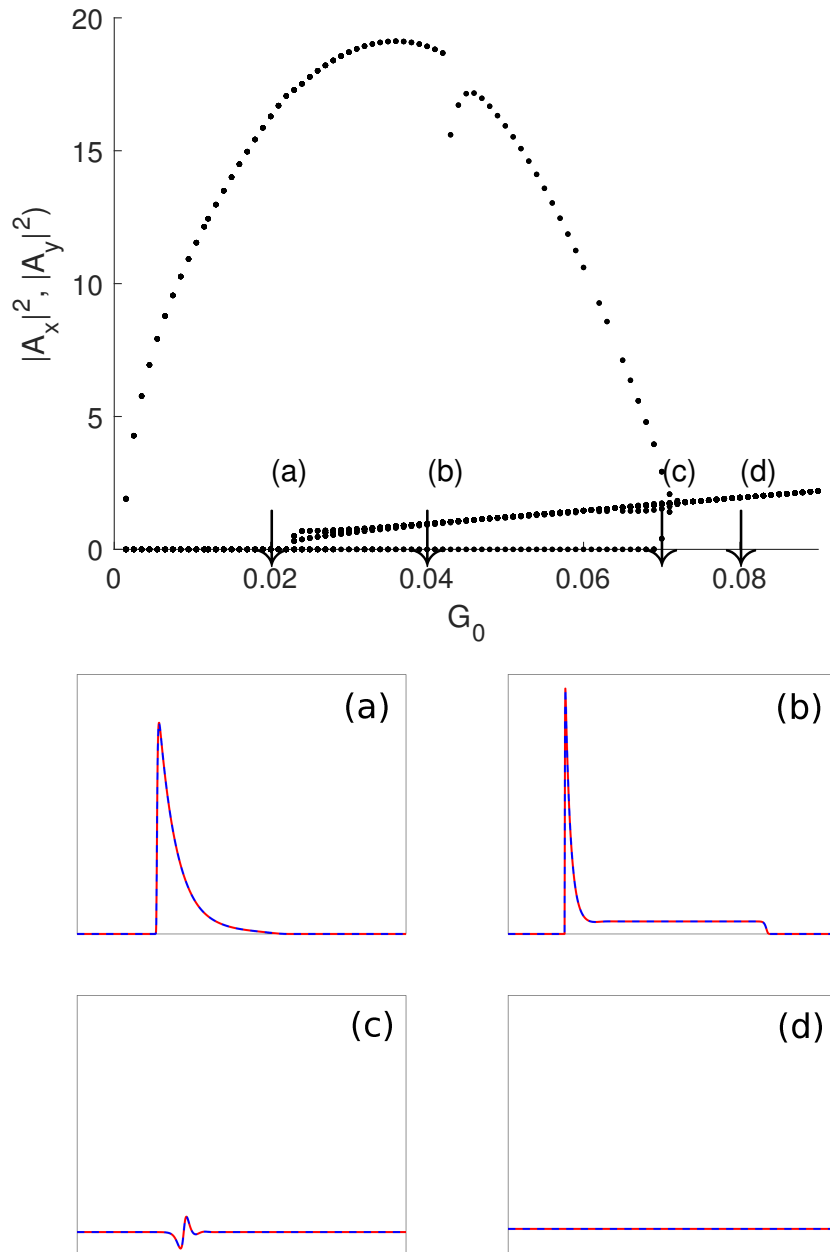


Figure 6: (color online) Top panel: Bifurcation diagram as a function of the gain chip pump for VECSEL with the same parameters as in Fig. 2 and initial conditions as in Fig. 3. The bottom panels present time traces of the intensities of x (red color) and y (blue color) linear polarizations at fixed values of G_0 as denoted in the bifurcation diagram.

the region of $G_0 \in [0.002, 0.023]$; time traces of the intensities of x and y polarizations for this case are shown in (a) in the bottom panel for $G_0 = 0.002$. With further increasing of G_0 the trailing edge of the mode-locked pulse develops a progressively increasing plateau - see the time traces for this case in (b) in the bottom panel for $G_0 = 0.004$. The amplitude of the pulses progressively decreases until the zero-intensity off-state disappears (it acquires a non-zero value). Time traces for this case is shown in (c) in the bottom panel for $G_0 = 0.007$. Finally, the VECSEL lases in CW regime with a constant intensity - see the time traces in (d) in the bottom panel for $G_0 = 0.008$.

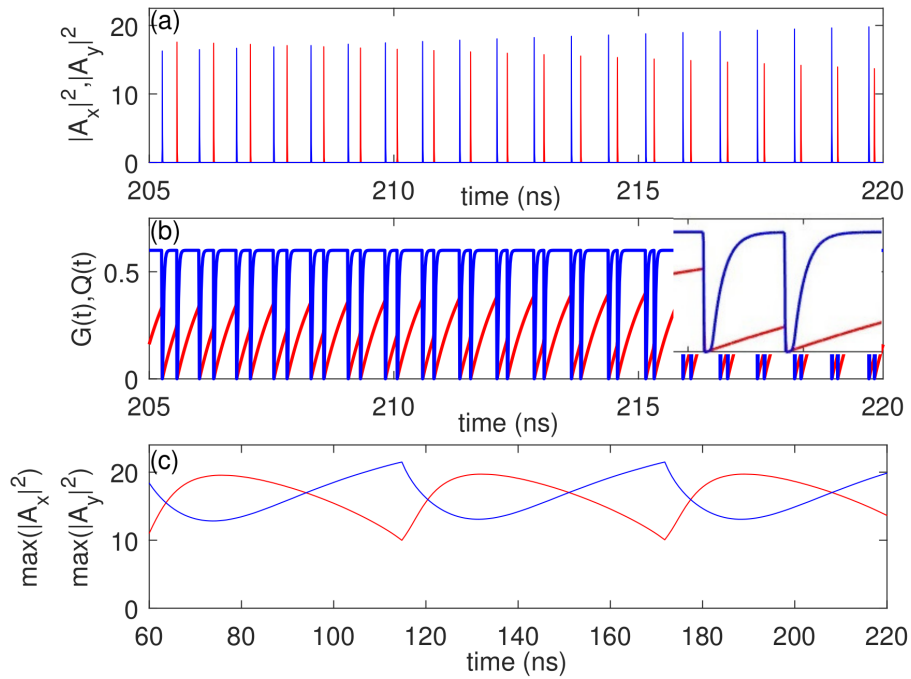


Figure 7: (color online) Same as Fig. 3 except that the VECSEL birefringence and the consequent optical path difference are considered, namely $\tilde{\gamma}_p = 0.25$ and $\tau_x = 75$ and $\tau_y = 76$. (a) Time traces of the intensities of x (red color) and y (blue color) linear polarizations; (b) time traces of G (red color), and Q (blue color) and (c) time traces of the maxima of the pulses in shown (a). The inset in (b) shows enlargement of region of $G(t)$, $Q(t)$ where two LP pulses are generated.

Next, we consider the presence of birefringence that may be due to the gain, the SA chips and/or can be deliberately introduced in the external cavity [8]. Optical birefringence appears due to refractive index anisotropy, which automatically means that the optical paths, and therefore the delay times τ_x and τ_y will be different. All this is accounted in Fig. 7 where we consider the case of $\tilde{\gamma}_p = 0.25$ and $\tau_x = 75$ and $\tau_y = 76$. Fig. 7(a) shows time traces of the intensities of x (red color) and y (blue color) linear polarizations. Remarkably, two pulse trains with orthogonal linear polarizations and slightly different repetition rate are observed. Because of this difference of the repetition rates, the LP pulses will overlap periodically (see e.g. the pulses at $t = 114ns$) and, as consequence, the amplitudes of the orthogonally polarized pulses will be periodically modulated. This is better evident in Fig. 7(c) where time traces of only the maxima of the pulses are shown. The reason for the modulation of the LP pulse amplitudes can be deduced from Fig. 7(b): when the LP pulses are well separated the gain G (the red curve) manages to partially recover after being sharply depleted at the first pulse - see also the inset of the figure. This recovery occurs less and less as the time difference between the two LP pulses diminishes and does not happen when the two LP pulses coincide.

The evolution of the light polarization is illustrated in Fig. 8 for the case of well separated in time consecutive pulses. As evident, light polarization remains linear during the mode-locked pulses, oriented along either the x or the y axis: the normalized Stokes parameter s_1 switches from -1 to $+1$ for the first and the second LP light pulses while s_2 and s_3 remain equal to zero during the pulses. However, for the case of overlapping pulses light polarization evolves in a continuous manner as shown in Fig. 9. In the region where the two pulses overlap, s_1 changes smoothly from -1 to $+0.2$. This change is accompanied by an increase of s_2 from 0 to almost 1 and a small increase of s_3 from 0 to about 0.05. This signifies that the light does not remain linearly polarized in the region of overlapping pulses: it turns its direction (signified by the large change of s_2 and acquires also a circular component

(signified by the non-zero value of s_3).

Finally, we illustrate the impact of the linewidth enhancement factors of the VECSEL gain chip and

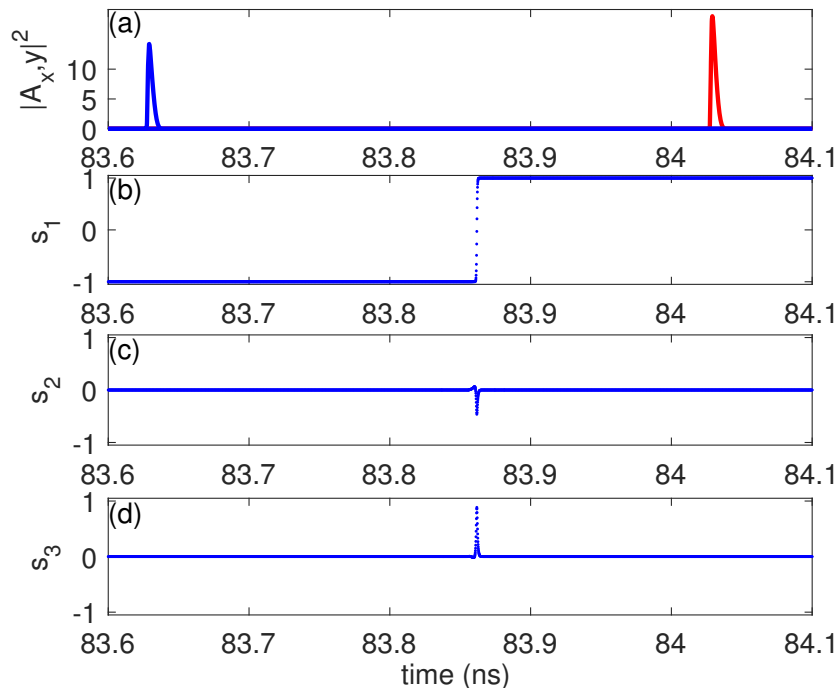


Figure 8: (color online) Evolution of the light polarization during a mode-locked pulse: (a) time traces of the intensities of x (red color) and y (blue color) linear polarizations; (b), (b) and (c) time traces of normalized Stokes parameters s_1 , s_2 and s_3 .

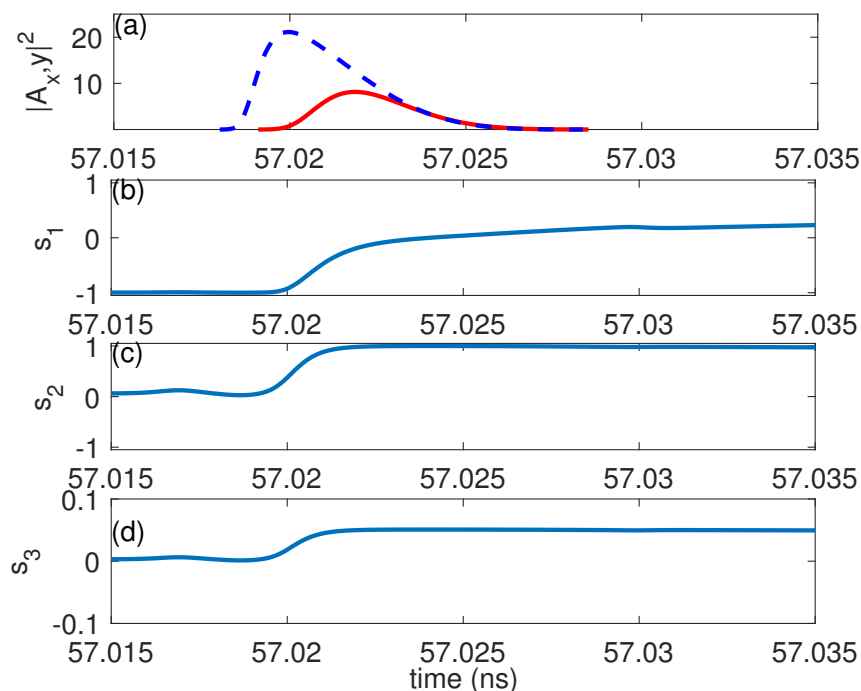


Figure 9: (color online) Evolution of the light polarization during a mode-locked pulse: (a) time traces of the intensities of x (red color) and y (blue color) linear polarizations; (b), (b) and (c) time traces of normalized Stokes parameters s_1 , s_2 and s_3 .

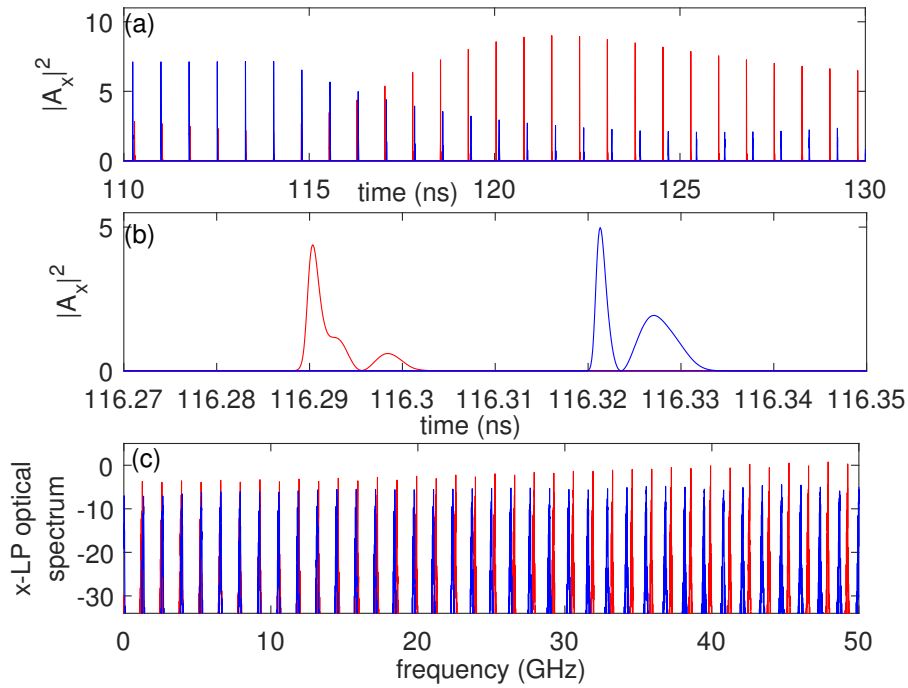


Figure 10: (color online) Same as Fig. 7 except that the linewidth enhancement factors of the VECSEL gain chip and saturable absorber are considered, namely $\alpha_g = 3$ and $\alpha_q = 1$. (a) Time traces of the intensities of x (red color) and y (blue color) linear polarizations; (b) time traces of single pulses in x (red color) and y (blue color) linear polarizations and (c) optical spectra for the x (red color) and y (blue color) LP light.

saturable absorber, namely $\alpha_g = 3$ and $\alpha_q = 1$. Fig. 10(a) presents the time traces of the intensities of x (red color) and y (blue color) linear polarizations and reveals similar sequences of pulses in the two linear polarizations with different repetition rate and modulated amplitude as already observed and explained for the case of zero linewidth enhancement factors. Fig. 10(b) shows the time traces of single pulses in x (red color) and y (blue color) linear polarizations and reveals that the trailing edges of the pulses are now distorted with more evident after-pulsing for the y -LP light. Fig. 10(c) presents the optical spectra for the x (red color) and y (blue color) polarizations, revealing two coexisting linearly polarized frequency combs with slightly different line spacing.

4 Conclusion

We have developed a spin-flip delay differential equation model for vertical external cavity lasers equipped with a saturable semiconductor absorber mirror. We obtained complete formulas for the anisotropy matrix and the associated field and carrier equations, providing a basis for a detailed study of the dynamics of the system. This model, based on the approximation of unidirectional generation in a ring cavity, is well suited to describe the mode-locking regimes involving two waves with different polarizations. Our analysis considers both phase and amplitude anisotropies in the laser cavity. In particular, the occurrence of optical birefringence due to refractive index anisotropy significantly affects the optical paths, thereby changing the cavity round-trip times for orthogonal linear polarizations.

We performed numerical simulations of the derived model equations. In our analysis, we examined the mode-locked solutions by studying their Stokes parameters and temporal behavior. Our results

revealed the presence of two distinct pulse trains with orthogonal linear polarizations and slightly different repetition rates. In the spectral domain, these operating regimes correspond to the generation of two optical frequency combs with slightly different line spacings due to the birefringence-induced time-of-flight difference.

References

- [1] M. Kuznetsov, F. Hakimi, R. Sprague, A. Mooradian. High-power (> 0.5 -W CW) diode-pumped vertical-external-cavity surface-emitting semiconductor lasers with circular TEM/sub 00/beams. *IEEE Photonics Technology Letters*, vol. 9, pp. 1063–1065, 1997.
- [2] E. A. Avrutin, J. H. Marsh, and E. L. Portnoi, Monolithic and multi-GHz mode locked semiconductor lasers: experiment, modeling and applications. *Proc. IEE Optoelectron.*, vol. 147, pp.251–278, 2000.
- [3] S. Hoogland, S. Dhanjal, A. C. Tropper, J.S. Roberts, R. Haring, R. Paschotta, F. Morier-Genoud, U. Keller. Passively Mode-Locked Diode-Pumped Surface-Emitting Semiconductor Laser, *Phot. Techn. Lett.*, vol. 12, pp. 1135–1137, 2000.
- [4] U. Keller, A. C. Tropper. Passively modelocked surface-emitting semiconductor lasers, *Phys. Reports*, vol. 429, pp. 67–120, 2006.
- [5] F. Emaury, A. Diebold, A. Klenner, C. J. Saraceno, S. Schilt, T. Südmeyer, U. Keller. Frequency comb offset dynamics of SESAM modelocked thin disk lasers, *Opt. Express*, vol. 23, pp. 21836–21856, 2015.
- [6] B. W. Tilma, M. Mangold, C. A. Zaugg, S. M. Link, D. Waldburger, A. Klenner, U. Keller. Recent advances in ultrafast semiconductor disk lasers, *Light: Science & Applications*, vol. 4, pp. e310–e310, 2015.
- [7] M. Gaafar, A. Rahimi-Iman, K. Fedorova, W. Stolz, E. Rafailov, M. Koch. Mode-locked semiconductor disk lasers, *Adv. Opt. Phot.*, vol. 8, pp. 370–400, 2016.
- [8] S. M. Link, A. Klenner, M. Mangold, C. A. Zaugg, M. Golling. B. W. Tilma, U. Keller, Dual-comb modelocked laser, *Opt. Exp.*, vol. 23, pp. 5521–5531, 2015.
- [9] A. G. Vladimirov, K. Panajotov, M. Tlidi. Orthogonally polarized frequency combs in a mode-locked VECSEL, *Opt. Lett.*, vol. 45, pp.252–255, 2020.
- [10] C. Castillo-Pinto, A. Broda, I. Sankowska, J. Muszalski, Y. Song, H. Zhang, K. Panajotov. Polarization dynamics of Vertical External-Cavity Surface-Emitting Laser with saturable absorber mirror, *Opt. Express*, vol. 30, pp. 47497–47504, 2022.
- [11] C. J. Chang-Hasnain, J. P. Harbison, G. Hasnain, A. C. Von Lehmen, L. T. Florez, and N. G. Stoffel. Polarization and transverse mode characteristics of vertical-cavity surface-emitting lasers, *IEEE J. Quantum Electron.*, vol. 27, pp. 1402–1408, 1991.
- [12] K. D. Choquette, D. A. Richie, and R. E. Leibenguth. Temperature dependence of gain-guided vertical-cavity surface-emitting laser polarization, *Appl. Phys. Lett.* **64**, 2062–2064 (1994)

- [13] T. Ackemann, M. Sondermann. Characteristics of polarization switching from the low to the high frequency mode in vertical-cavity surface-emitting lasers, *Appl. Phys. Lett.*, **78**, 3574–3576 (2001).
- [14] K. Panajotov, F. Prati. Polarization Dynamics of VCSELs, ch.6 in *VCSELs*, R. Michalzik (ed), New York, NY, USA: Springer Ser. Opt. Sciences, vol. 166, pp. 181–232, 2013.
- [15] M. Virte, K. Panajotov, H. Thienpont and M. Sciamanna. Deterministic polarization chaos from a laser diode, *Nature Photonics*, vol. 7, pp.60–65, 2013.
- [16] K. Panajotov, M. Sciamanna, M. Arizaleta, H. Thienpont. Optical Feedback in Vertical-Cavity Surface-Emitting Lasers, *IEEE J. Sel. Top. Quant. Electr.*, vol. 19, pp. 1700312–1700312, 2013.
- [17] M. Sciamanna, K. Panajotov. Two-mode injection locking in vertical-cavity surface-emitting lasers, *Opt. Lett.*, vol. 30, 2903–2905, 2005.
- [18] E. Averlant, M. Tlidi, H. Thienpont, T. Ackemann, K. Panajotov. Vector cavity solitons in broad area Vertical-Cavity Surface-Emitting Lasers, *Sci. Reports*, vol. 6, 20428, 2016.
- [19] K. Panajotov, M. Tlidi, Localized chaos of elliptically polarized cavity solitons in broad-area VCSEL with a saturable absorber. *Opt. Lett.*, vol. 43, pp. 5663–5666, 2018.
- [20] M. Lindemann, G. Xu, T. Pusch, R. Michalzik, M. R. Hofmann, I. Zutic, N. C. Gerhardt. Ultrafast spin-lasers, *Nature*, vol. 568, 212–215, 2019.
- [21] M. San Miguel, Q. Feng, J. V. Moloney. Light-polarization dynamics in surface-emitting semiconductor laser, *Phys. Rev. A*, vol. 52, pp. 1728–1739, 1995.
- [22] J. Martin-Regalado, F. Prati, M. San Miguel, N. B. Abraham. Polarization Properties of Vertical-Cavity Surface-Emitting Lasers, *IEEE J. Quant. Electr.*, vol. 33, pp. 765–783, 1997.
- [23] X. Hachair, G. Tissoni, H. Thienpont, K. Panajotov. Linearly polarized bistable localized structure in a medium size vertical-cavity surface-emitting laser, *Phys. Rev. A*, vol. 79, 011801(R), 2009.
- [24] A. G. Vladimirov, D. Turaev. Model for passive mode locking in semiconductor lasers, *Phys. Rev. A*, vol. 72, 033808, 2005.
- [25] A. Gahl, S. Balle, M. San Miguel. Polarization dynamics of optically pumped VCSELs, *IEEE J. Quantum Electron.*, vol. 35, pp. 342–351, 1999.
- [26] R. Al-Seyab, D. Alexandropoulos, I. D. Henning, M. J. Adams. Instabilities in Spin-Polarized Vertical-Cavity Surface-Emitting Lasers, *IEEE Photonics Journal*, vol. 3, pp. 799–809, 2011.